Late glycolysis supplies energy for effector trafficking in Magnaporthe oryzae, implicating a potential target in managing rice blast

Zhengguang Zhang

zhgzhang@njau.edu.cn

Nanjing Agricultural University https://orcid.org/0000-0001-8253-4505

Xinyu Liu

Nanjing Agricultural University

Ju Shen

Nanjing Agricultural University

Zanfeng Li

Nanjing Agricultural University

Chen Chen

Nanjing Agricultural University

Lingbo Shen

Nanjing Agricultural University

Yangjie He

Nanjing Agricultural University

Ziqian Guo

Nanjing Agricultural University

Jiayun Xu

Nanjing Agricultural University

Miao Wu

Nanjing Agricultural University

Ping Yang

Nanjing Agricultural University

Leiyun Yang

Nanjing Agricultural University

Muxing Liu

Nanjing Agricultural University

Gang Li

Nanjing Agricultural University

Haifeng Zhang

Nanjing Agricultural University

Ping Wang

Louisiana State University Health Sciences Center New Orleans

---

Article

Keywords:

Posted Date: January 15th, 2024

DOI: https://doi.org/10.21203/rs.3.rs-3833043/v1

Additional Declarations: There is **NO** Competing Interest.

Abstract

During the early stages of the *Magnaporthe oryzae* and rice interaction, rice generates reactive oxygen species (ROS) burst to inhibit further proliferation of the pathogen. At the same time, *M. oryzae* secretes various effectors into the host through vesicle trafficking that subverts ROS stress. However, how these effectors are secreted in a timely manner remains unclear. Here, we found that vesicle movement significantly increases under ROS stress and that glycolysis is the energy source for such effector trafficking. Specifically, ROS inhibits the palmitoylation of glyceraldehyde-3-phosphate dehydrogenase (GAPDH) that inhibits GAPDH-mediated phase separation, and resulting raised pool of GAPDH in the cytoplasm facilitates ATP generation required for vesicle trafficking. To ensure GAPDH-mediated glycolysis, a Nudix hydrolase, MoNud5, catalyzes nicotinamide adenine dinucleotide + hydrogen (NADH) for maintaining GAPDH activities *in vivo*. To explore whether inhibiting *M. oryzae* GAPDH activities effectively controls rice blast, we discovered a small molecule, TH287, that inhibits the pathogenesis of *M. oryzae.* TH287 binds to MoNud5 to inhibit its function, resulting in increased NADH and decreased GAPDH activities. Our studies reveal the significance of glycolysis-mediated vesicle trafficking in the blast fungus and provides evidence that GAPDH suppression is a potential strategy to control rice blasts.

Introduction

Given their sessile lifestyles, plants confront multiple abiotic and biotic stresses that result in heavy losses to agricultural production (Kadota et al., 2015; Oldroyd, 2013; Sies et al., 2017; Zipfel and Oldroyd, 2017). To defend against extracellular pathogens, plants primarily depend on diverse innate immunity strategies, including the respiratory burst NADPH oxidase (RBOH)-mediated ROS, Pathogen-Associated Molecular Pattern (PAMP)-triggered immunity (PTI), and Effector-Triggered Immunity (ETI) (Kadota et al., 2015; Zhou and Zhang, 2020).

The hemibiotrophic fungus *Magnaporthe oryzae* and monocotyledonous rice (*Oryza sativa L*) serve as an important pathogen-host interaction and effector function model (Wilson and Talbot, 2009; Zhang et al., 2016). Rice blast is a devastating crop disease with significant economic importance, leading to hundreds of millions of grain losses worldwide. Defense against blast is characterized by strong responses, including ROS accumulation and callose deposition (Giraldo and Valent, 2013; Liu and Zhang, 2021; Park et al., 2012; Park et al., 2016). However, pathogens can sense host immune responses and react by initiating the secretion of numerous effector proteins that subvert plant immunity (Kawasaki et al., 1997; Lanfranco et al., 2005; Liu and Zhang, 2021; Molina and Kahmann, 2007). Recent studies showed that host-derived ROS induces global transcriptional reprogramming of the virulence genes in *M. oryzae*. For instance, it activates MoOsm1-mediated pathways to activate the downstream transcription factor MoAtf1, which in turn induces the transcription of various effector genes to boost virulence (Guo et al., 2010; Liu et al., 2020). Additionally, the translational regulation of *M. oryzae* genes plays a critical role in subverting plant immunity. Under ROS stress, heat-shock protein MoHsp70s, together with MoYvh1, are accumulated in the nucleus to facilitate ribosome maturation, subsequently enhancing the synthesis of effector proteins (Liu et al., 2016; Liu et al., 2018). Previous studies also showed that numerous

pathogen-derived proteins are secreted to prevent the activation of the unfolded protein response (UPR) pathway (Yin et al., 2019). For efficient trafficking of secretory proteins, *M. oryzae* operates a delicate sorting system to transport effectors (Qian et al., 2022; Tang et al., 2015). Still, the mechanism by which *M. oryzae* orchestrates vesicle trafficking, including the energy source under ROS-related stress, remains unclear.

Vesicle trafficking is mediated by the molecular motors dynein and kinesin that transport cargo over long distances (Hirokawa et al., 2010; Morikawa et al., 2022). As the dynein and kinesin motors require ATP to transport cargo, vesicle trafficking is an energy-consuming process. For rapid trafficking, *M. oryzae* must have enough energy sources for these molecular motors to function. However, the energy supply under ROS stress is unclear. In eukaryotic cells, glycolysis and tricarboxylic acid cycle (TCA) are the major donors of energy (Ames, 2000). The process of glucose breakdown within the cytosol is orchestrated by the glycolysis pathway, a pivotal metabolic pathway which divided into two distinct stages. The early stage, often referred to the energy consumption stage, lays the groundwork for generating phosphorylated active substrates vital for subsequent processes. As glycolysis progresses beyond this preparatory phase and arrives at the glyceraldehyde-3-phosphate dehydrogenase (GAPDH)-mediated oxidation of glyceraldehyde-3-phosphate, it marks a critical turning point. At this stage, high-energy phosphate bonds are generated, signaling the transition into the second stage, also called the "energy release stage." Here, the pathway culminates in the production of pyruvate, accompanied by the liberation of free energy and the formation of reducing NADH, crucial components in cellular energy production. Compared to the relatively low energy conversion efficiency, TCA and subsequent oxidative phosphorylation in mitochondria produce a large amount of ATP (Ames, 2000). How ATP is distributed during the interaction between *M. oryzae* and rice and is continuously provided to facilitate vesicle trafficking during effector secretion is not clear.

Here, we examined the contribution of glycolysis to ATP supply required for vesicle trafficking during *M. oryzae* and rice interaction upon ROS stress.

Results

ROS accelerates glycolysis-dependent vesicle trafficking

To evaluate vesicle trafficking under ROS stress, we monitored the dynamics of Rab GTPase MoRab5, an important molecular switch in regulating intracellular membrane trafficking of early endocytosis by promoting early endosomal fusion and motility, which is generally used to label vesicles in *M. oryza*e (Ramanujam et al., 2013). MoRab5 was fused with GFP (MoRab5-GFP) and transformed into *M. oryzae*. The transformants were treated with 5 mM H_2O_2, and Rab5-GFP was monitored in mycelia using Video Spot Tracker. The movement of MoRab5 is faster, and the speed is increased over 2-fold under ROS stress (Fig. 1A and 1C). This observation was confirmed in infection, as K23-Guy11, a moderate resistance cultivar-strain interaction, exhibited fewer and more restricted lesions with massive ROS accumulation compared to the susceptible LTH-Guy11 (Liu et al., 2018; Yin et al., 2019). MoRab5-labelled

vesicle dynamics revealed faster movements in K23-Guy11 than in LTH-Guy11 (Fig. 1B and 1D). These results demonstrated that vesicle trafficking is accelerated upon ROS perception.

Vesicle trafficking processes, including tethering and fusion, require a high energy supply. To investigate the energy utilization mechanism of vesicle movement, we first examined the ATP levels in *M. oryzae* under ROS stress. ATP increased drastically after H_2O_2 treatment (Fig. S1A). Then, we took advantage of a genetically encoded fluorescent sensor Perceval to monitor the ATP:ADP ratio in living cells and found that the signal of Perceval polarized from CFP to RFP upon ATP binding (Werley et al., 2020). By using this system, we were able to observe that ATP formed patches. However, this pattern disappeared, and ATP patches scattered into tiny dots coordinating with more co-localization with MoRab5 when treated with H_2O_2 (Fig. 1E). To further evaluate the localization of ATP during infection, primary infecting hyphae (IH) of the wild-type strain Guy11 were observed and ATP exhibited as a series spot in the IH of rice cultivar K23, but not in the susceptible LTH cultivar in which the localization of ATP is plaque-like (Fig. 1F). Taken together, these results suggested that there is a rapid increase and displacement of ATP in response to ROS stress.

Glycolysis, TCA cycle, and the subsequent oxidative phosphorylation process are critical for the generation of ATP. To investigate ATP donors, we tested whether oligomycin, which blocks mitochondria ATP production (Chang and Reynolds, 2006), or the GAPDH inhibitor iodoacetate (Matthews et al., 1997), affects vesicle trafficking under ROS stress. Both oligomycin and iodoacetate significantly reduced ATP levels in *M. oryzae*, which could not be rescued by ROS stress (Fig. S1B). The results, using the vesicle trafficking inhibitor Brefeldin A (BFA) as a control, indicated that despite causing a decrease in vesicular trafficking rate, vesicle movement still increased by 2 ~ fold in response to ROS stress after co-treatment with oligomycin and H_2O_2 for 30 min, whereas the vesicle movement did not accelerate in the presence of iodoacetate (Fig. 1G and 1H). These results indicated that GAPDH-mediated glycolysis is critical for the induction of vesicle movement in response to ROS stress.

ROS inhibits the liquid-like phase of GAPDH

To further understand the mechanisms by which GAPDH facilitates vesicle movement, we analyzed the relative activity of glycolysis under ROS stress. The relative activity of glycolysis in mycelia was significantly induced after 15 or 30 min H_2O_2 treatment (Fig. 2A). Since the transcripts and protein amount of MoGapdh did not change after H_2O_2 treatment (Fig. S2), we then examined the enzyme activity of MoGapdh. The GAPDH activity was induced after H_2O_2 treatment for 15 min (Fig. 2B), suggesting that the enhanced enzyme activity may be important for its positive regulation of ROS response. In addition to assessing the activity of GAPDH, we also examined the activity of other glycolysis proteins, including hexokinase, phosphoglycerate kinase, and pyruvate kinase, under ROS exposure. The results indicated that there were no significant changes in the activity of these enzymes when treated with H_2O_2 (Fig. S3).

Although GAPDH is mainly cytosolic, it was reported to be in specific subcellular compartments, including the cytoskeleton, membranes, and nuclei (Tristan et al., 2011). In *M. oryzae*, we noticed that MoGapdh was distributed throughout the cell; however, various large, immobile foci were observed in the cytoplasm (Fig. 2C). Of note, the number of foci in mycelia were significantly reduced to 30% after H_2O_2 treatment for 30 minutes (Fig. 2C and 2E). Additionally, the foci in *M. oryzae*-infected K23 were fewer than those in *M. oryzae*-infected LTH, with K23 having higher ROS accumulation than LTH (Fig. 2D and 2E). These results indicated that ROS alters the localization of MoGapdh.

Previous studies showed that proteins might form giant foci and often undergo a liquid–liquid phase separation (LLPS) (Fujioka et al., 2020). To determine whether these large and immobile foci of MoGapdh exhibit LLPS characteristics, we performed fluorescence recovery after photobleaching (FRAP) *in vivo*. Post-photobleaching, ~ 80% of the MoGapdh-GFP signal recovered over time (Fig. 2F). We further used 1,6-hexanediol, which dissolves LLPS condensates by disrupting hydrophobic interactions, to treat the mycelia of *M. oryzae*. Following 1,6-hexanediol treatment, the sizes of the MoGapdh-GFP foci were drastically fewer (Fig. 2G). To further distinguish these foci from vesicles, we used MoRab5-RFP to mark the vesicles *in vivo*. The result showed that MoGapdh-GFP foci were not co-localized with vesicles (Fig. 2H). Used MoAtg8 as marker, we observed MoGapdh was not localized to vacuoles, which is also not being degraded under nitrogen starvation treatment (Fig. S4). Together, these results demonstrate that MoGapdh undergoes LLPS *in vivo*.

Palmitoylation of GAPDH is critical for GAPDH-mediated phase separation

GAPDH is mainly localized in the cytosol, but it has also been reported to be localized in some intracellular compartments, such as membranes and vesicles, due to partial palmitoylation (Tristan et al., 2011). We therefore examined the palmitoylation status of MoGapdh and whether this status would change under ROS stress. Palmitoylated GAPDH was detected. Of note, ROS inhibits the palmitoylation of MoGapdh and this modification was significantly decreased at 30 min post-treatment (Fig. 3A). By predicting the candidate palmitoylated sites through GPS-Palm (Ning et al., 2021), we generated a mutant form of MoGapdh, MoGapdh^{C4S}, by mutating cysteine (C) to serine (S). The palmitoylation status was determined through a parallel palmitoylation assay with or without the hydroxylamine thioester-cleavage step, and the levels of palmitoylation of MoGapdh^{C4S} were remarkably reduced (Fig. 3B). Additionally, the LLPS feature of MoGapdh foci was significantly reduced by MoGapdh^{C4S} (Fig. 3C), indicating MoGapdh palmitoylation is critical for its LLPS formation

As the palmitoylation may function on enhancing membrane affinity, we hypothesized that this modification may cause the accumulation of MoGapdh on the vesicle membrane. Although the aggregation on vesicles is not obvious during microscopic examination (Fig. S5A and S5B), we examined MoGapdh that is not located inside the vesicle through Z-stack image analysis (Supplementary Video1 and Video 2). In addition, the Western blot assay showed that MoGapdh is induced on vesicles when treated with H_2O_2 for 30 min (Fig. S5C). Consistent with this observation, the MoGapdh^{C4S} mutant

accumulated higher levels of MoGapdh than the wild-type strain (Fig. S5D). By further using 100 and 500 mM NaCl incubating to break the electrovalent bond, the majority of MoGapdh is dissociated from the vesicle after 500 mM NaCl treatment (Fig. 3D), indicating that MoGapdh is accumulated on the surface of the vesicle.

We further hypothesize that the accumulation of MoGapdh on the vesicle could provide ATP for its movement. We found that the activity of MoGapdh located on vesicles was significantly induced on the vesicle after H_2O_2 treatment in the MoGapdh^{C4S} mutant compared to the control sample (Fig. 3E). Additionally, it is known that GAPDH is in a complex with two other glycolytic enzymes, 3-phosphoglycerate kinase (PGK) and pyruvate kinase (PK) (Srivastava and Bernhard, 1986), and generates ATP by using NAD + as a substrate. To validate this, we first isolated vesicles and performed Western blot assays that showed vesicle locations of PKG and PK (Fig. S6). We also measured ATP production by incubating vesicles with GAP, ADP, Pi, and NAD, and significant GAP-dependent ATP production was observed under H_2O_2 treatment in the MoGapdh^{C4S} strain (Fig. 3F). These results suggested that GAPDH is enzymatically active around vesicles upon ROS stress.

Inhibition of GAPDH blocks the apoplastic effector secretion in M. oryzae

Since GAPDH is critical for providing energy for vesicle transport during *M. oryzae* infection, we tested whether the GAPDH inhibitor iodoacetate is effective in controlling *M. oryzae.* In the detached barley infection assay, conidial suspensions with 1 nM, 10 nM, 0.1 μM, 1 μM, and 10 μM iodoacetate were dropped onto barley leaves, and the results were photographed after 5 days. The results showed that iodoacetate inhibits *M. oryzae* growth on barley. Even at the lower concentration of 10 nM, iodoacetate could fully inhibit virulence (Fig. 4A). In addition, when conidial suspensions (1×10^5 spores/ml) supplemented with 10 nM iodoacetate were infiltrated into the sheath of 4-week-old rice seedlings, at 36 hpi, iodoacetate caused Type II and Type III IH, while Guy11 without iodoacetate produced more invasive Type III and Type IV IH (Fig. 4B and 4C). We further generated the deletion mutant of *MoGAPDH* through homologous recombination and assessed the GAPDH activity in this mutant (Fig. S7E and 7F). Notably, the Δ*Mogapdh* mutant exhibited a complete inability to produce conidia (Fig. S7C and S7D). To investigate its impact on pathogenicity, we conducted infection using mycelium agar blocks on both barley and rice leaves. The results revealed that Δ*Mogapdh* led to significant defects in the pathogenicity of *M. oryzae* (Fig. S7A and S7B). Given the multifaceted nature of GAPDH as a moonlighting protein with diverse roles, we also generated an inactivation strain of MoGapdh by targeting the glyceraldehyde 3-phosphate binding sites (Fig. S8A). This site-specific mutation resulted in severe defects on the vegetative growth, conidiation, and pathogenicity (Fig. S8B, S8C and S8D).

We further investigate the role of MoGapdh in effector secretion. To achieve this, we generated multiple silenced strains with reduced GAPDH expression, which resulted in a reduction in conidial production (Fig. S9A and S9B). Nevertheless, we inoculated rice leaves with conidial suspensions from each of these silenced strains. After a 7-day incubation, we observed the formation of small, restricted lesions, indicating the significant role of MoGapdh in the pathogenicity of *M. oryzae* (Fig. 4D). Previous work

showed two distinct secretory pathways for effector delivery during plant infection by the rice blast fungus including the conventional fungal ER-Golgi secretion pathway responsible for secreting apoplastic effectors, and a separate pathway for cytoplasmic effectors, reliant on exocyst components Exo70 and Sec5 for efficient secretion. Within these secretory pathway, fungal cytoskeleton is important for conventional effector secretion as evidenced by impaired secretion observed upon treating with BFA or LatA (Giraldo et al., 2013). We thus examined vesicle movement in Guy11 with and without iodoacetate. At 0.1 μM, the vesicle movement was significantly decreased (Fig. 4E). The vesicle movement of RNAi-*MoGAPDH* was also evaluated and found to be inhibited under ROS stress (Fig. 4F). Moreover, we examined the localization of apoplastic effectors MoSlp1-GFP during Guy11 infection with iodoacetate or infection with RNAi-*MoGAPDH* strains. The localization of MoSlp1-GFP was altered by iodoacetate, and they were not localized to the expected EIHM region, suggesting that iodoacetate inhibits the apoplastic secretion (Fig. 4G and 4H). Taken together, these results indicated that inhibition of GAPDH blocks the apoplastic secretion in *M. oryzae*.

We further tested whether this inhibition can be explored as a putative fungicide to control *M. oryzae* infection. We first examined host-derived ROS levels by 3, 3’-diaminobenzidine (DAB) staining and 2',7'-dichlorodihydrofluorescein diacetate (H2DCFDA), an oxidative stress indicator, at 24 hpi. When treated with iodoacetate, the IH-infected host cells were not stained by DAB, as no reddish-brown precipitate was seen (Fig. S10A and S10B). This suggested that the inhibitor may also suppress ROS accumulation near the infection sites. We also used H2DCFDA to detect ROS accumulation during infection. The hyphae failed to be strained by H2DCFDA under iodoacetate treatment (Fig. S10C). These results indicated that iodoacetate may cause defects on the host-derived immunity during infection. ROS burst is a potent PTI response triggered by multiple PAMPs (Kadota et al., 2015; Kadota et al., 2014), so flg22/chitin-triggered ROS production was examined using a luminol-based assay. As shown in Figure S10D and S10E, PAMPs-triggered ROS burst in rice protoplasts was suppressed when treated with iodoacetate. Based on these results, we speculated that iodoacetate also inhibits OsGAPDH resulting in a defect in ROS immunity. Indeed, the activity of OsGAPDH (Os08g0126300) was significantly decreased when treated with iodoacetate (Fig. S10F).

NUDIX hydrolase hydrolyzes NADH to rescue GAPDH activities

The effect of iodoacetate suppressing OsGAPDH implies that it cannot be used as a putative fungicide. We then explored other approaches of indirectly inhibiting GAPDH activities. GAPDH catalyzes glyceraldehyde-3-phosphate to produce D-glycerate 1,3-bisphospate and NADH, which is a reversible process. Therefore, we hypothesized that the excess production of NADH may have a catabolic repression effect. To test this, we first measured NAD + and NADH contents *in vivo*. When treated with H_2O_2 for 30 min, the rate of NADH/(NAD + + NADH) was decreased (Fig. 5A). We then co-incubated NADH of various concentrations with GAPDH for 30 min and found that NADH inhibited GAPDH activities at high concentrations (Fig. 5B), suggesting excessive NADH inhibits the catalytic activity of GAPDH.

The nucleoside diphosphate linked moiety X (NUDIX) hydrolase family proteins hydrolyze pyrophosphates, including NADH (Xu et al., 2004). We performed an HmmerSearch to identify 18 Nudix hydrolase homologs from *M. oryzae*. We then checked the transcript levels of these hydrolases during infection with and without H_2O_2 treatment, and found only MGG_08699 (*MoNUD5*) and MGG_08378 (*MoNUD3*) were upregulated during the early stage of infection (Fig. S11A and S11B). A previous study showed that ROS induces the phosphorylation of the transcriptional factor MoAtf1 to activate the transcription of various genes in the oxidoreduction pathways (Liu et al., 2020). Among these genes, we found MoAtf1 binds to the promoter of *MoNUD5* but not *MoNUD3* (Fig. S12A and S12B). In addition, we found that only the expression of *MoNUD5* was induced in MoAtf1^{S124D} (transcription activated strain) (Fig. S12C), indicating MoNud5 might be important in linking ROS responses to NADH levels.

To reveal the functions of MoNud5 in regulating NADH, we tested the hydrolase activity of MoNud5 using a series of nucleotide derivatives as the substrates. As shown in Fig. 5C, MoNud5, but not the enzyme activity dead mutant, MoNud5^{ED}, could hydrolyze ADPR, NADH, and FLAVIN. We also co-incubated MoNud5 in various concentrations with 0.8 mM NADH and MoGapdh, and found that MoNud5 rescued the inhibition of NADH on GAPDH (Fig. 5D).

MoNud5 deletion reduces M. oryzae apoplastic effector secretion

As MoNud5 regulates NADH that affects GAPDH activity, we generated the deletion mutant of *MoNUD5* and examined whether deletion of MoNud5 affects effector secretion in *M. oryzae*. We first examined the vegetative growth of the Δ*Monud5* mutant on complete medium (CM) and minimal medium (MM), the mutant exhibited no defects on vegetative growth after incubation at 28°C for 7 d in the dark (Fig. S13). In conidial suspension spray assays, we first observed that the lesion areas were decreased by nearly 60% when infected with the Δ*Monud5* mutant, in comparison to the WT and complemented mutant strains (Fig. 6A and 6C). In addition, conidial suspensions (1×10^5 spores/ml) were also infiltrated into the sheath of 4-week-old rice seedlings. The Δ*Monud5* mutant caused fewer and more restricted lesions than the control, and the mutant phenotype was rescued in the complemented (Fig. 6B and 6D). These results indicated that MoNud5 is required for full virulence of *M. oryzae.*

To test whether MoNud5 inhibits the host immune response, we examined ROS production by rice sheath DAB staining. ROS was rarely observed in leaves infected with Guy11 and the complemented strain but highly accumulated in leaves infected by the Δ*Monud5* mutant (Fig. 6E and 6F). We then detected the activity of MoGapdh in the mutant under ROS stress, and the result showed no changes in MoGapdh activities when treated with H_2O_2 for 30 min (Fig. S14A). As GAPDH functions to generate ATP, we detected the localization of ADP/ATP in the Δ*Monud5* mutant by transducing fluorescent sensor Perceval. The result showed that vesicles specifically co-localize with ADP under ROS stress (Fig. S14B), suggesting that Δ*Monud5* is defective in ADP to ATP conversion. We also tested whether MoNud5 functions on GAPDH-mediated vesicle trafficking and found that vesicle trafficking is inhibited under ROS stress in K23-Guy11 pairing (Fig. S14C and S14D). Finally, we extracted the extracellular fluid from MoSlp1-GFP strain and found that the secretion of MoSlp1 in the Δ*Monud5* mutant was inhibited

(Fig. 6G and 6H). These results indicated that MoNud5 is important for apoplastic effector secretion in *M. oryzae*.

TH287 specifically inhibits MoNud5 activities

MoNud5 is a homolog of the mammalian Nudix hydrolase MTH1, and a phylogenetic analysis revealed that MoNud5 shares a highest homology with rice OsJ05P01700 (Fig. S15). Previous studies found that MTH1 can be inhibited by several small molecules, including TH287 (Gad et al., 2014). MoNud5 could also be the specific target for these inhibitors. We found that the hydrolase activity of MoNud5 was significantly decreased by TH287 at 10 μM (Fig. 7B). We then performed an MST assay and found a stronger binding affinity between TH287 and MoNud5 than TH287 and OsJ05P01700 (Fig. 7A and S16). To examine whether TH287 can be used as an antifungal compound, we carried out a preventive effect test under three treatment conditions, including co-treatment with spores, pre-treatment for 24 hours, and post-treatment after 24 hours of infection. The results showed that co-treatment has the best controlling effect, followed by pre-treatment, and then post-treatment (Fig. 7C and 7D).

As TH287 does not appear to affect the vegetative growth of *M. oryzae* (Fig. S17A), we evaluated its effect on *M. oryzae.* TH287 caused defects in conidiation and appressorium formation of *M. oryzae* (Fig. S17B and S17C). Infection assays on rice sheaths revealed that TH287 significantly inhibits IH growth (Fig. S18A). Additionally, the DAB staining assay showed that TH287 inhibits the ability of *M. oryzae* to scavenge host ROS (Fig. S18B), similar to what we observed in the Δ*Monud5* mutant. These results indicated that TH287 could be used as a potential fungicide to control rice blasts.

Discussion

The ROS burst upon pathogen infection is a hallmark of plant immune responses. In response to host-derived ROS, pathogens synthesize and secrete numerous effector proteins to circumvent host immunity (Doehlemann and Hemetsberger, 2013; Liu et al., 2018). Defects in effector secretion by vesical trafficking cause excessive effector accumulation, ultimately leading to ER stress and compromised pathogenicity. Therefore, a robust vesicle trafficking machinery is critical for the pathogen response to ROS. However, the mechanism, including energy supplies, by which pathogens orchestrate their vesicle trafficking remains not fully understood. In this study, we discovered that *M. oryzae* facilitates vesicle trafficking under ROS stress by providing more energy through glycolysis. ROS dissociates GAPDH from LLPS by inhibiting the palmitoylation of GAPDH, raising the GAPDH-pool in the cytoplasm and the vesicles. This result in more ATP accumulating around vesicles to speed up their trafficking. We further revealed that the Nudix hydrolase MoNud5 hydrolyzes NADH to enhance GAPDH activities and, ultimately, glycolysis. In addition, we identified TH287 as an inhibitor of the Nudix hydrolase, suggesting its feasibility as a new class of fungicides (Fig. 8).

Previous work showed two distinct secretory pathways for effector delivery during plant infection by the rice blast fungus including the conventional fungal ER-Golgi secretion pathway responsible for secreting apoplastic effectors, and a separate pathway for cytoplasmic effectors, reliant on exocyst components

Exo70 and Sec5 for efficient secretion. Within these secretory pathway, fungal cytoskeleton is important for conventional effector secretion as evidenced by impaired secretion observed upon treating with BFA or LatA (Giraldo et al., 2013; Li et al., 2023a). Similarly, our result demonstrated that silencing *MoGAPDH* or treatment with IA caused the defects on the secretion of apoplastic effectors (Fig. 4G and 4H), indicating that GAPDH mediated energy supply is important for the conventional secretion pathway. By contrast, cytoplasmic effectors are secreted by a different pathway involving the exocyst complex, remaining unaffected by BFA treatment. In addition, a recent work showed that unconventionally secreted effectors requiring tRNA wobble U34 thiolation carry signal peptides, likely traverse the Golgi-bypass pathway(Li et al., 2023a). These results demonstrated that the secretion of cytoplastic effector is independent to cytoskeleton, however, we noticed that silence of *MoGAPDH* or treatment with IA also caused the defects on the cytoplastic effectors (Fig. S19). As a fundamental process to maintain the homeostasis of membrane-enclosed organelles in eukaryotic cells, vesicle trafficking pathway includes vesicle formation from the donor membrane, vesicle transport, and vesicle fusion with the target membrane. Expect for the intracellular vesicle transport relies on a cytoskeletal track, which involves motor proteins and energy, the tethering to the plasma membrane for subsequent membrane fusion of secretory vesicle also requires energy consumption (Cui et al., 2022). The formation of the SNARE complex provides the energy necessary for driving membrane fusion through four-helix bundles and fusion pore formation (Gao et al., 2012; He and Wu, 2007). Considering the additional energy needed for the pore formation and dilation, one SNARE complex may be only sufficient for lipid exchange between two membranes, a greater energy input is needed for a complete fusion event (Hernandez et al., 2012; Sinha et al., 2011). Therefore, in addition to the involvement of multiple SNARE complexes in providing energy, the energy generated by this GAPDH may also be involved in the timely transport of cytoplasmic effectors.

TCA cycle in the mitochondria is an efficient energy generation strategy (Ames, 2000). Although the pathogen can still respond to ROS stress and accelerate vesicle transport rate under oligomycin treatment, impaired TCA cycle also caused a significant decrease in vesicle transport rate and defects on the pathogenicity of *M. oryzae* (Fig. 1H and S20). Recent research has highlighted the significance of α-ketoglutarate, a TCA derivative derived from glutaminolysis, in reactivating TOR signaling and sustaining biotrophic growth, underscoring the critical role of the TCA cycle in the infection process *M. oryzae* (Li et al., 2023b). Why glycolysis, an inefficient energy generation pathway, but not TCA cycle provides the energy source in response to ROS of *M. oryzae*? Previous studies in mammalian models showed that mitochondria provide most of the energy consumed in the brain, however, mitochondria are not evenly distributed within the neurons, and are most abundant at sites with a high-energy demand (MacAskill and Kittler, 2010). When signals travel between neurons, a large number of vesicles were produced for neurotransmitter transport. Zala et al. found that glycolytic enzymes located on vesicles rather than mitochondria are critical to maintaining the high vesicular velocities that are characteristic of fast axonal transport, indicating that glycolytic enzymes can be accumulated spatially to regulate the signaling transport (Zala et al., 2013). Here, our results suggested that glycolysis is spatiotemporal in response to external signals. In comparison to the station-kept mitochondria, glycolysis provides energy for greater

mobility, which can quickly provide energy for cellular processes such as efficient vesicle trafficking under ROS stress. On the other, TCA cycle provided basic energy metabolism for the biotrophic growth of *M. oryzae*.

Notably, previous studies showed that several enzymes, including phosphoglucose isomerase, hexokinase, and glucokinase in early glycolysis are dispensable for biotrophic growth in rice and disease development (Fernandez et al., 2014; Zhang et al., 2011). The glycolytic pathway can be dissected into two pivotal stages: the energy consumption stage (early phase) and the energy liberation stage (late phase). Throughout the energy-consuming phase, glucose molecules undergo a series of transformations, culminating in the conversion into glyceraldehyde 3-phosphate while concurrently consuming ATP. Given that this phase sets the stage for subsequent reactions, it is conceivable that various alternative pathways, such as glucose-6-phosphatase-mediated gluconeogenesis and the pentose phosphate pathway, influenced by transketolase, can serve as viable substitutes for glycolysis, thereby generating energy when glycolytic function is compromised (Bian et al., 2022; TeSlaa et al., 2023). When glycolysis advances to the oxidation of 3-phosphate glyceraldehyde, resulting in the formation of 1,3-diphosphoglycerate catalyzed by GAPDH, it signifies the initiation of the later stage of glycolytic metabolism, primarily aimed at energy release. In mammals, any disruptions occurring within this intricate process involving GAPDH, phosphoglycerate kinase, or pyruvate kinase can lead to severe deficiencies. In our present study, we deliberately generated deletion mutants of *MoGAPDH* and *MoPGK1* in the phytopathogenic fungus *M. oryzae*. Through our observations, we have ascertained that these mutants exhibit distinct defects in both their developmental processes and pathogenic capabilities, as exhibited in Figure S21A. These findings raise the possibility that the observed divergence from the early glycolytic pathway may stem from the absence of functional substitutes during the energy release phase, emphasizing the essential role of late glycolysis in facilitating the pathogenicity of the rice blast fungus. Also in mammalian cells, GAPDH localizes on vesicles via a huntingtin-dependent mechanism that functions on the transportation of FAT within axons (Burke et al., 1996; Chaudhary et al., 2021). However, as no huntingtin protein was identified in fungi, how GAPDH provides energy for vesicles remains unclear.

Our study also found that MoGapdh forms LLPS condensates that significantly decrease under ROS stress (Fig. 2C-2G). Previous studies suggested that LLPS condensate formation occurs in three different ways: (i) folded proteins with well-defined interaction surfaces can form oligomers that engender multivalency of other associative patches, which participate in stereospecific interactions; (ii) folded domains can be strung together by flexible linkers to generate linear multivalent proteins; and (iii) intrinsically disordered regions (IDRs) can serve as scaffolds for multiple, distinctive short linear motifs (Andersen et al., 2005; Boke et al., 2016; Fong et al., 2013). We found that MoGapdh contains both IDR regions and interaction sites to form oligomers by itself. However, blocking the formation of oligomerization bonds by DTT treatment causes defects in the formation of LLPS (Fig. S22), indicating that the LLPS condensate formation of GAPDH is dependent on interaction surfaces. Besides interaction surfaces, protein palmitoylation is also important for the LLPS of MoGapdh (Fig. 3C). Protein palmitoylation is a reversible lipid post-translational modification catalyzed by the zinc finger protein family. Given that palmitoylation enhances the hydrophobicity of specific protein subdomains and can

confer changes in protein stability, localization, protein-protein interaction, and signal transduction (Ko and Dixon, 2018), it is possible that the removal of palmitoylation of MoGapdh decreases its hydrophobicity, resulting in reduced entropy that promotes dissociation of LLPS. In our study, we observed no significant accumulation of MoGapdh in vesicles. We speculated that dissociated LLPS provides the free form of MoGapdh that evenly distributes in the cytoplasm to raise GAPDH-pool levels around the vesicles. The increase in the total amount of free GAPDH in the cytoplasm, in turn, increases the energy supply for vesicular transport under ROS stress.

Finally, most current fungicides target mainly ergosterol biosynthesis, melanin biosynthesis, β-tubulin assembly, and others (Hawkins and Fraaije, 2018). However, along with the long-term application of fungicides, some of the targets are prone to mutations, leading to a rapid development of fungicide resistance. New targets for the fungicide are urgently needed. As GAPDH produces D-glycerate 1,3-bisphospate with NADH is a reversible process (Tristan et al., 2011), the overproduction of NADH inhibit the occurrence of this reaction. We speculated that raising the content of NADH *in vivo* may control glycolysis activity and showed that deletion of *MoNUD5* led to an increase of NADH that, in turn, suppresses the activity of GAPDH and the pathogenicity of *M. oryzae* (Fig. 5D and 6). To examine whether the mammalian Nudix hydrolase inhibitor MTH1 is effective against MoNud5, we provided evidence demonstrating that TH287 is effective in controlling *M. oryzae* infection. The differentiated inhibition ability of MTH1 MoNud5 and rice Nudix hydrolases could be further explored for the purpose of developing it as an alternative fungicide to control rice blasts.

Materials and Methods

Strains and cultural conditions

M. oryzae Guy11 strain was used as the wild-type (WT) strain in this study. All of the mentioned strains were maintained on the complete medium (CM) for 3–15 days at 28°C in the dark (Liu et al., 2016; Talbot et al., 1993). For conidia production, strains were cultured on straw decoction and corn (SDC) (100 g straw, 40 g corn powder, 15 g agar in 1 L of distilled water) agar media for one week at 28°C in the dark before 3 days of black light illumination (Qi et al., 2016). The liquid CM media was used to culture mycelia with or without additional treatment for protein, RNA, and DNA extractions.

Targeted gene deletion and transformation

The standard one-step gene replacement strategy was adopted to generate the *MoGAPDH* and *MoNUD5* gene deletion mutants. First, PCR was used to amplify two fragments with 1.0 kb of sequences flanking the targeted gene by primer pairs. The PCR products ligated with the hygromycin-resistance cassette (*HPH*) released from the vector pCX62 followed by digested with restriction endonucleases (Fig. S21B). Ultimately, the recombinant constructs were sequenced. We amplified and transformed the 3.4 kb fragment, including the HPH cassette and the flanking sequences into the Guy11 strain protoplasts. To verified the mutant, verification primers are designed to amplify internal probes (probe 1) and external probes (probe 2) (Fig. S21B), and putative mutants were screened by PCR (Fig. S21C). Fragments for

mutant complementation were amplified by PCR and inserted into the vector pYF11 followed by transformation into the mutant strain protoplasts through PEG-mediated transformation.

Infection assays and ROS observation

For the virulence test, conidia were suspended to a concentration of 5 x 10^4 spores/ml in a 0.2% (w/v) gelatin solution, and 4 ml each was sprayed on two-week-old rice seedlings (Oryza sativa CO39). Inoculated plants were kept in a growth chamber at 25°C with 90% humidity and in the dark for the first 24 hours, followed by a 16/8 hours light/dark cycle. The disease severity was assessed at 7 days after inoculation. For observation of the penetration and invasive growth in rice cells, conidial suspensions (1×10^5 spores/ml) were injected into the leaf sheath. At 28°C for 24 or 48 hours, the inner epidermis of infected sheaths was observed under a microscope. To observe ROS derived from rice, rice leaves or sheaths were stained with DAB (Sigma-Aldrich) as described.

For the measurement of ROS levels, leaves were cut into discs with a cork borer and pre-incubated overnight in sterile-distilled water. After flg22 or chitin treatment, ROS production was monitored by the luminol chemiluminescence assay (Liu et al., 2019).

Microscale Thermophoresis (MST) analysis

Based on the structure prediction of Alphafold2, we screening a 3D small molecular library from Pubchem (https://ftp.ncbi.nlm.nih.gov/pubchem/Compound_3D/10_conf_per_cmpd/SDF/), and identified a series small molecular including TH187. Binding reactions of recombinant GST-MoNud5 and its homolog in rice with Th287 or other inhibitors were measured by MST in a Monolith NT.Label Free (Nano Temper Technologies GMBH) instrument. Labeled HIS-MoNud5 (10 μM) was displaced by a buffer containing. TH287 or other inhibitors in the assay buffer was incubated with labeled protein (1:1, v/v) for 10 min. Free standard capillaries and measured with 20% LED power and 40% MST power. The KD Fit function of the Nano Temper Analysis Software (Version 1.5.41) was used to fit the curve and calculate the value of the dissociation constant (Kd).

Epifluorescence microscopy

M. oryzae cells expressing fluorescent protein-fused chimera were incubated under appropriate conditions. Epifluorescence microscopy was performed using the microscope Zeiss LSM980, 63x water. MoRab5-GFP was introduced into transformants to mark the vesicles. To examine the effects of Brefeldin A (sigma) on vesicle movement, we prepared the stock solution of BFA, 10mg/ml, in dimethylsulphoxide (DMSO, sigma). The concentration used is 50μg/ml and treated for 5h before observed. For FRAP assay. Regions containing MoGapdh-GFP were selected for photo-bleaching. The photobleaching was carried out using an Argon-multiline laser at a wavelength of 488 nm with 70% laser power and 150 iterations in ROI. Images were acquired with 2% laser power at a wavelength of 488 nm every 5 sec. For quantitative analyses, fluorescence intensity was measured using the ZEISS ZEN blue software for the FRAP experiment, recoveries were measured as fluorescence intensity of photobleached area normalized to the

intensity of the same area before bleaching. Analysis of the recovery curves was performed with FIJI/ImageJ.

Palmitoylation assay.

The palmitoylation assays were performed as previously described (Li et al., 2017). Generally, Strains transduced with GFP-tagged proteins were homogenized in lysis buffer containing 50 mM Tris (PH 7.5), 150 mM NaCl, 0.5% Triton-X 100, and 1x protease inhibitor for 1 h on ice. After centrifuged at 20,000×g for 15 min at 4°C, 50 mM N-ethylmaleimide was added for blocking free sulfhydryl groups, and proteins were then immunoprecipitated using Anti-GFP-Agarose beads at 4°C overnight. The beads were then washed three times with lysis buffer and eluted with glycine The eluted proteins were divided into two equal parts: one treated with 1 M hydroxylamine and the other with 1M Tris·HCl as control in the presence of activated thiol-Sepharose 4B. One hour later, the sepharose beads were washed three times with lysis buffer without protease inhibitor at room temperature and then resuspended in PBS buffer and heated at 100°C for 10 min. Palmitoylated proteins were detected by Western blots.

GAPDH-dependent ATP production

Five micrograms of the purified vesicles were resuspended in 200 µl of reaction buffer (20 mM HEPES-KOH, pH 7.2, 200 mM sucrose, 50 mM KCl, 1 mM NAD, 0.5 mM ADP, and 1 mM KH_2PO_4). To measure ATP production, 1 mM glyceraldehyde-3-phosphate(G3P) was added. The reaction was incubated at room temperature for 1 min, and then, 100 µl of the reaction mixture were detected by ATP Assay Kit (Beyotime, S0026) in a 96-well plate. After 10 min, luminescence was recorded as described (Liu et al., 2022).

Declarations

Acknowledgments

The authors declare that there is no conflict of interest.

References

1. Ames, A., 3rd (2000). CNS energy metabolism as related to function. Brain research. Brain research reviews *34*, 42-68.
2. Andersen, J.S., Lam, Y.W., Leung, A.K., Ong, S.E., Lyon, C.E., Lamond, A.I., and Mann, M. (2005). Nucleolar proteome dynamics. Nature *433*, 77-83.
3. Bian, X., Jiang, H., Meng, Y., Li, Y.P., Fang, J., and Lu, Z. (2022). Regulation of gene expression by glycolytic and gluconeogenic enzymes. Trends in cell biology *32*, 786-799.
4. Boke, E., Ruer, M., Wühr, M., Coughlin, M., Lemaitre, R., Gygi, S.P., Alberti, S., Drechsel, D., Hyman, A.A., and Mitchison, T.J. (2016). Amyloid-like self-assembly of a cellular compartment. Cell *166*, 637-650..

5. Burke, J.R., Enghild, J.J., Martin, M.E., Jou, Y.S., Myers, R.M., Roses, A.D., Vance, J.M., and Strittmatter, W.J. (1996). Huntingtin and DRPLA proteins selectively interact with the enzyme GAPDH. Nature medicine *2*, 347-350.
6. Chang, D.T., and Reynolds, I.J. (2006). Mitochondrial trafficking and morphology in healthy and injured neurons. Progress in neurobiology *80*, 241-268.
7. Chaudhary, S., Dhiman, A., Patidar, A., Malhotra, H., Talukdar, S., Dilawari, R., Chaubey, G.K., Modanwal, R., Raje, C.I., and Raje, M. (2021). Moonlighting glyceraldehyde-3-phosphate dehydrogenase (GAPDH) modulates protein aggregation. Biochimica et biophysica acta. Molecular basis of disease *1867*, 166202.
8. Cui, L., Li, H., Xi, Y., Hu, Q., Liu, H., Fan, J., Xiang, Y., Zhang, X., Shui, W., and Lai, Y. (2022). Vesicle trafficking and vesicle fusion: mechanisms, biological functions, and their implications for potential disease therapy. Molecular biomedicine *3*, 29.
9. Doehlemann, G., and Hemetsberger, C. (2013). Apoplastic immunity and its suppression by filamentous plant pathogens. The New phytologist *198*, 1001-1016.
10. Fernandez, J., Marroquin-Guzman, M., and Wilson, R.A. (2014). Evidence for a transketolase-mediated metabolic checkpoint governing biotrophic growth in rice cells by the blast fungus *Magnaporthe oryzae*. PLoS pathogens *10*, e1004354.
11. Fong, K.W., Li, Y., Wang, W., Ma, W., Li, K., Qi, R.Z., Liu, D., Songyang, Z., and Chen, J. (2013). Whole-genome screening identifies proteins localized to distinct nuclear bodies. The Journal of cell biology *203*, 149-164.
12. Fujioka, Y., Alam, J.M., Noshiro, D., Mouri, K., Ando, T., Okada, Y., May, A.I., Knorr, R.L., Suzuki, K., Ohsumi, Y.*, et al.* (2020). Phase separation organizes the site of autophagosome formation. Nature *578*, 301-305.
13. Gad, H., Koolmeister, T., Jemth, A.S., Eshtad, S., Jacques, S.A., Ström, C.E., Svensson, L.M., Schultz, N., Lundbäck, T., Einarsdottir, B.O.*, et al.* (2014). MTH1 inhibition eradicates cancer by preventing sanitation of the dNTP pool. Nature *508*, 215-221.
14. Gao, Y., Zorman, S., Gundersen, G., Xi, Z., Ma, L., Sirinakis, G., Rothman, J.E., and Zhang, Y. (2012). Single reconstituted neuronal SNARE complexes zipper in three distinct stages. Science (New York, N.Y.) *337*, 1340-1343.
15. Giraldo, M.C., Dagdas, Y.F., Gupta, Y.K., Mentlak, T.A., Yi, M., Martinez-Rocha, A.L., Saitoh, H., Terauchi, R., Talbot, N.J., and Valent, B. (2013). Two distinct secretion systems facilitate tissue invasion by the rice blast fungus *Magnaporthe oryzae*. Nature Communications *4*, 1996.
16. Giraldo, M.C., and Valent, B. (2013). Filamentous plant pathogen effectors in action. Nature Reviews Microbiology *11*, 800-814.
17. Guo, M., Guo, W., Chen, Y., Dong, S., Zhang, X., Zhang, H., Song, W., Wang, W., Wang, Q., Lv, R.*, et al.* (2010). The basic leucine zipper transcription factor Moatf1 mediates oxidative stress responses and is necessary for full virulence of the rice blast fungus *Magnaporthe oryzae*. Molecular plant-microbe interactions:MPMI *23*, 1053-1068.

18. Hawkins, N.J., and Fraaije, B.A. (2018). Fitness penalties in the evolution of fungicide resistance. Annual review of phytopathology *56*, 339-360.
19. He, L., and Wu, L.G. (2007). The debate on the kiss-and-run fusion at synapses. Trends in neurosciences *30*, 447-455.
20. Hernandez, J.M., Stein, A., Behrmann, E., Riedel, D., Cypionka, A., Farsi, Z., Walla, P.J., Raunser, S., and Jahn, R. (2012). Membrane fusion intermediates via directional and full assembly of the SNARE complex. Science (New York, N.Y.) *336*, 1581-1584.
21. Hirokawa, N., Niwa, S., and Tanaka, Y. (2010). Molecular motors in neurons: transport mechanisms and roles in brain function, development, and disease. Neuron *68*, 610-638.
22. Kadota, Y., Shirasu, K., and Zipfel, C. (2015). Regulation of the NADPH oxidase RBOHD during plant immunity. Plant & cell physiology *56*, 1472-1480.
23. Kadota, Y., Sklenar, J., Derbyshire, P., Stransfeld, L., Asai, S., Ntoukakis, V., Jones, J.D., Shirasu, K., Menke, F., Jones, A.*, et al.* (2014). Direct regulation of the NADPH oxidase RBOHD by the PRR-associated kinase BIK1 during plant immunity. Molecular cell *54*, 43-55.
24. Kawasaki, L., Wysong, D., Diamond, R., and Aguirre, J. (1997). Two divergent catalase genes are differentially regulated during *Aspergillus nidulans* development and oxidative stress. Journal of bacteriology *179*, 3284-3292.
25. Ko, P.J., and Dixon, S.J. (2018). Protein palmitoylation and cancer. EMBO report *19*, e46666
26. Lanfranco, L., Novero, M., and Bonfante, P. (2005). The mycorrhizal fungus *Gigaspora margarita* possesses a CuZn superoxide dismutase that is up-regulated during symbiosis with legume hosts. Plant physiology *137*, 1319-1330.
27. Li, G., Dulal, N., Gong, Z., and Wilson, R.A. (2023a). Unconventional secretion of *Magnaporthe oryzae* effectors in rice cells is regulated by tRNA modification and codon usage control. Nature microbiology *8*, 1706-1716.
28. Li, G., Gong, Z., Dulal, N., Marroquin-Guzman, M., Rocha, R.O., Richter, M., and Wilson, R.A. (2023b). A protein kinase coordinates cycles of autophagy and glutaminolysis in invasive hyphae of the fungus *Magnaporthe oryzae* within rice cells. Nature communications *14*, 4146.
29. Li, W., Li, W., Zou, L., Ji, S., Li, C., Liu, K., Zhang, G., Sun, Q., Xiao, F., and Chen, D. (2017). Membrane targeting of inhibitory Smads through palmitoylation controls TGF-β/BMP signaling. Proceedings of the National Academy of Sciences of the United States of America *114*, 13206-13211.
30. Liu, X., Gao, Y., Guo, Z., Wang, N., Wegner, A., Wang, J., Zou, X., Hu, J., Liu, M., and Zhang, H. (2022). Molug4 is a novel secreted effector promoting rice blast by counteracting host OsAHL1-regulated ethylene gene transcription. *235*, 1163-1178.
31. Liu, X., Qian, B., Gao, C., Huang, S., Cai, Y., Zhang, H., Zheng, X., Wang, P., and Zhang, Z. (2016). The putative protein phosphatase MoYvh1 functions upstream of MoPdeH to regulate the development and pathogenicity in *Magnaporthe oryzae*. Molecular plant-microbe interactions : MPMI *29*, 496-507.
32. Liu, X., Yang, J., Qian, B., Cai, Y., Zou, X., Zhang, H., Zheng, X., Wang, P., and Zhang, Z. (2018). MoYvh1 subverts rice defense through functions of ribosomal protein MoMrt4 in *Magnaporthe oryzae*. PLoS

pathogens *14*, e1007016.

33. Liu, X., and Zhang, Z. (2021). A double-edged sword: reactive oxygen species (ROS) during the rice blast fungus and host interaction. The FEBS journal *289*, 5505-5515
34. Liu, X., Zhou, Q., Guo, Z., Liu, P., Shen, L., Chai, N., Qian, B., Cai, Y., Wang, W., Yin, Z.*, et al.* (2020). A self-balancing circuit centered on MoOsm1 kinase governs adaptive responses to host-derived ROS in *Magnaporthe oryzae*. eLife *9*, e61605
35. MacAskill, A.F., and Kittler, J.T. (2010). Control of mitochondrial transport and localization in neurons. Trends in cell biology *20*, 102-112.
36. Matthews, R.T., Ferrante, R.J., Jenkins, B.G., Browne, S.E., Goetz, K., Berger, S., Chen, I.Y., and Beal, M.F. (1997). Iodoacetate produces striatal excitotoxic lesions. Journal of neurochemistry *69*, 285-289.
37. Molina, L., and Kahmann, R. (2007). An *Ustilago maydis* gene involved in H_2O_2 detoxification is required for virulence. The Plant cell *19*, 2293-2309.
38. Morikawa, M., Jerath, N.U., and Ogawa, T. (2022). A neuropathy-associated kinesin KIF1A mutation hyper-stabilizes the motor-neck interaction during the ATPase cycle. *41*, e108899.
39. Ning, W., Jiang, P., Guo, Y., Wang, C., Tan, X., Zhang, W., Peng, D., and Xue, Y. (2021). GPS-Palm: a deep learning-based graphic presentation system for the prediction of S-palmitoylation sites in proteins. Briefings in bioinformatics *22*, 1836-1847.
40. Oldroyd, G.E. (2013). Speak, friend, and enter: signalling systems that promote beneficial symbiotic associations in plants. Nature reviews. Microbiology *11*, 252-263.
41. Park, C.H., Chen, S., Shirsekar, G., Zhou, B., Khang, C.H., Songkumarn, P., Afzal, A.J., Ning, Y., Wang, R., Bellizzi, M.*, et al.* (2012). The *Magnaporthe oryzae* effector AvrPiz-t targets the RING E3 ubiquitin ligase APIP6 to suppress pathogen-associated molecular pattern-triggered immunity in rice. The Plant cell *24*, 4748-4762.
42. Park, C.H., Shirsekar, G., Bellizzi, M., Chen, S., Songkumarn, P., Xie, X., Shi, X., Ning, Y., Zhou, B., Suttiviriya, P.*, et al.* (2016). The E3 Ligase APIP10 connects the effector AvrPiz-t to the NLR receptor Piz-t in rice. PLoS pathogens *12*, e1005529.
43. Qi, Z., Liu, M., Dong, Y., Zhu, Q., Li, L., Li, B., Yang, J., Li, Y., Ru, Y., Zhang, H.*, et al.* (2016). The syntaxin protein (MoSyn8) mediates intracellular trafficking to regulate conidiogenesis and pathogenicity of rice blast fungus. The New phytologist *209*, 1655-1667.
44. Qian, B., Su, X., Ye, Z., Liu, X., Liu, M., Shen, D., Chen, H., and Zhang, H. (2022). MoErv29 promotes apoplastic effector secretion contributing to virulence of the rice blast fungus *Magnaporthe oryzae*. The New phytologist *233*, 1289-1302.
45. Ramanujam, R., Calvert, M.E., Selvaraj, P., and Naqvi, N.I. (2013). The late endosomal HOPS complex anchors active G-protein signaling essential for pathogenesis in magnaporthe oryzae. PLoS pathogens *9*, e1003527.
46. Sies, H., Berndt, C., and Jones, D.P. (2017). Oxidative Stress. Annual review of biochemistry *86*, 715-748.

47. Sinha, R., Ahmed, S., Jahn, R., and Klingauf, J. (2011). Two synaptobrevin molecules are sufficient for vesicle fusion in central nervous system synapses. Proceedings of the National Academy of Sciences of the United States of America *108*, 14318-14323.
48. Srivastava, D.K., and Bernhard, S.A. (1986). Enzyme-enzyme interactions and the regulation of metabolic reaction pathways. Current topics in cellular regulation *28*, 1-68.
49. Talbot, N.J., Ebbole, D.J., and Hamer, J.E. (1993). Identification and characterization of MPG1, a gene involved in pathogenicity from the rice blast fungus *Magnaporthe grisea*. The Plant cell *5*, 1575-1590.
50. Tang, W., Ru, Y., Hong, L., Zhu, Q., Zuo, R., Guo, X., Wang, J., Zhang, H., Zheng, X., Wang, P.*, et al.* (2015). System-wide characterization of bZIP transcription factor proteins involved in infection-related morphogenesis ofMagnaporthe oryzae. Environmental Microbiology *17*, 1377-1396.
51. TeSlaa, T., Ralser, M., Fan, J., and Rabinowitz, J.D. (2023). The pentose phosphate pathway in health and disease. Nature metabolism *5*, 1275-1289.
52. Tristan, C., Shahani, N., Sedlak, T.W., and Sawa, A. (2011). The diverse functions of GAPDH: views from different subcellular compartments. Cellular signalling *23*, 317-323.
53. Werley, C.A., Boccardo, S., Rigamonti, A., Hansson, E.M., and Cohen, A.E. (2020). Multiplexed Optical Sensors in Arrayed Islands of Cells for multimodal recordings of cellular physiology. *11*, 3881.
54. Wilson, R.A., and Talbot, N.J. (2009). Under pressure: investigating the biology of plant infection by *Magnaporthe oryzae*. Nature reviews. Microbiology *7*, 185-195.
55. Yin, Z., Feng, W., Chen, C., Xu, J., Li, Y., Yang, L., Wang, J., Liu, X., Wang, W., Gao, C.*, et al.* (2019).
56. Shedding light on autophagy coordinating with cell wall integrity signaling to govern pathogenicity of *Magnaporthe oryzae*. Autophagy *16*, 900-916.
57. Zala, D., Hinckelmann, M.V., Yu, H., Lyra da Cunha, M.M., Liot, G., Cordelières, F.P., Marco, S., and Saudou, F. (2013). Vesicular glycolysis provides on-board energy for fast axonal transport. Cell *152*, 479-491.
58. Zhang, H., Zheng, X., and Zhang, Z. (2016). The *Magnaporthe grisea* species complex and plant pathogenesis. Molecular plant pathology *17*, 796-804.
59. Zhang, L., Lv, R., Dou, X., Qi, Z., Hua, C., Zhang, H., Wang, Z., Zheng, X., and Zhang, Z. (2011). The function of MoGlk1 in integration of glucose and ammonium utilization in *Magnaporthe oryzae*. PloS one *6*, e22809.
60. Zhou, J.M., and Zhang, Y. (2020). Plant Immunity: Danger Perception and Signaling. Cell *181*, 978-989.
61. Zipfel, C., and Oldroyd, G.E. (2017). Plant signalling in symbiosis and immunity. Nature *543*, 328-336.

Figures

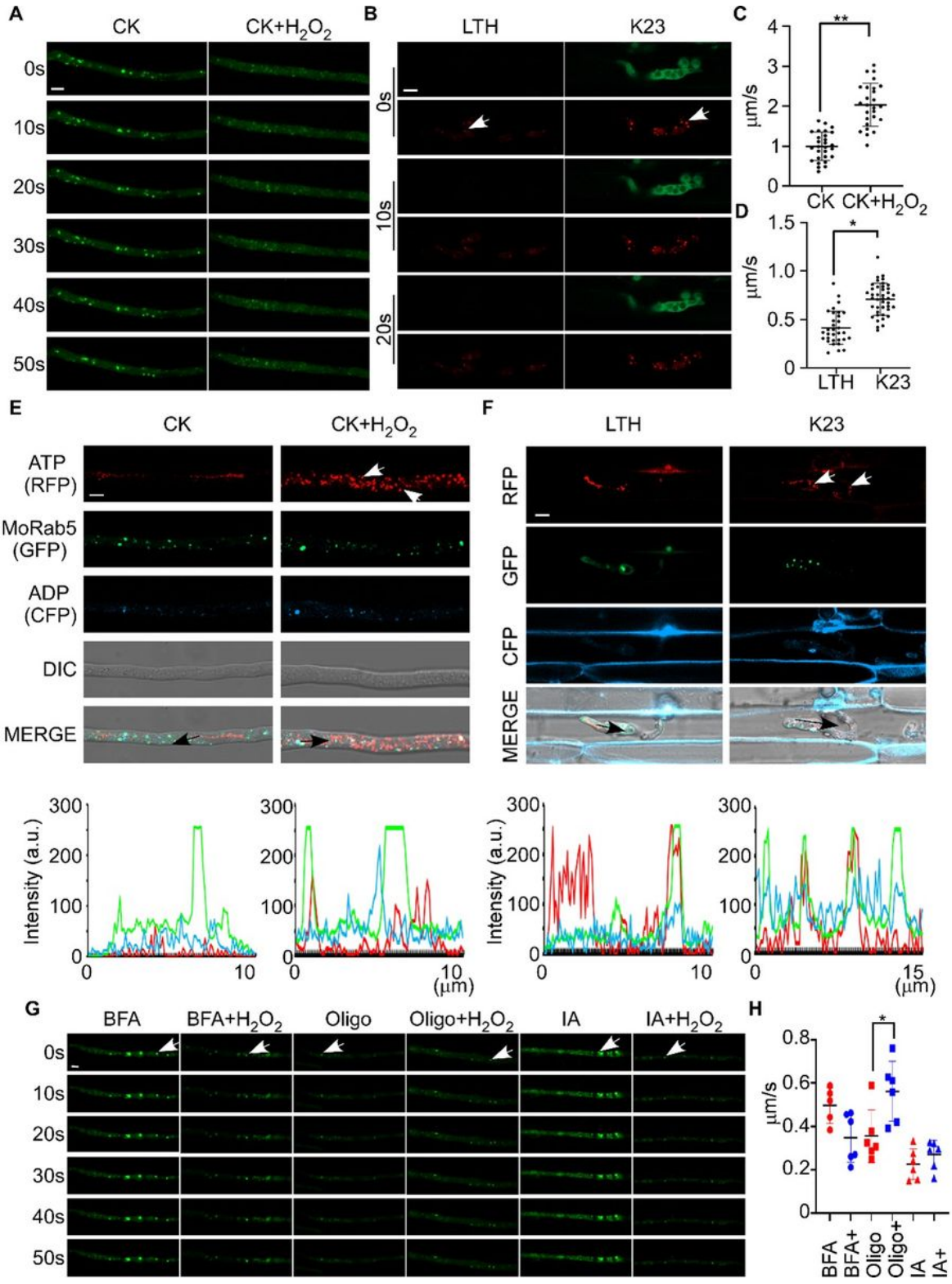

Figure 1

ROS facilitates vesicle trafficking in *M. oryzae*.

(A) Time-lapse images of cells expressing the MoRab5-GFP reporter at different time intervals treated with or without H_2O_2. Scale bar = 10 μm. CK represents ddH_2O treatment. (B) Time-lapse images *M. oryzae* expressing MoRab5-RFP in rice cells. The conidial suspension of Guy11 (1 x 10^5 spores/ml) was

inoculated in the excised rice sheath of 4-week-old rice seedlings of LTH and K23. The invasive hyphae growth was stained by H2DCFDA (GFP channel) and observed at 24 hpi. White arrows represent Rab5 spots. (C) and (D) The movement rates of Rab5-labeled vesicles were detected using Video Spot Tracker in mycelium and infection hyphae cells. Error bars represent standard deviation, "*", $P< 0.05$, "**" $P< 0.01$. (E) and (F) Localization of ATP (RFP) and ADP (CFP) was observed under ROS stress in mycelium and infection hyphae. ATP/ADP sensor PercevalHR was transduced into *M. oryzae*. CK represents ddH_2O treatment. White arrows represent dissociated dots under ROS stress. MoRab5-GFP represents vesicles. Scale bar = 5 μm. (G) Time-lapse images of cells expressing the vesicle reporter MoRab5 at different time intervals treated with oligomycin (Oligo) and iodoacetic acid (IA) with or without H_2O_2 treatment. The vesicle trafficking inhibitor Brefeldin A (BFA) was used as control, white arrows represent Rab5 spots. Scale bar = 5 μm. (I) Video Spot Tracker analyzed the movement of vesicles under oligomycin or iodoacetic acid with ROS treatment. "*", $P< 0.05$.

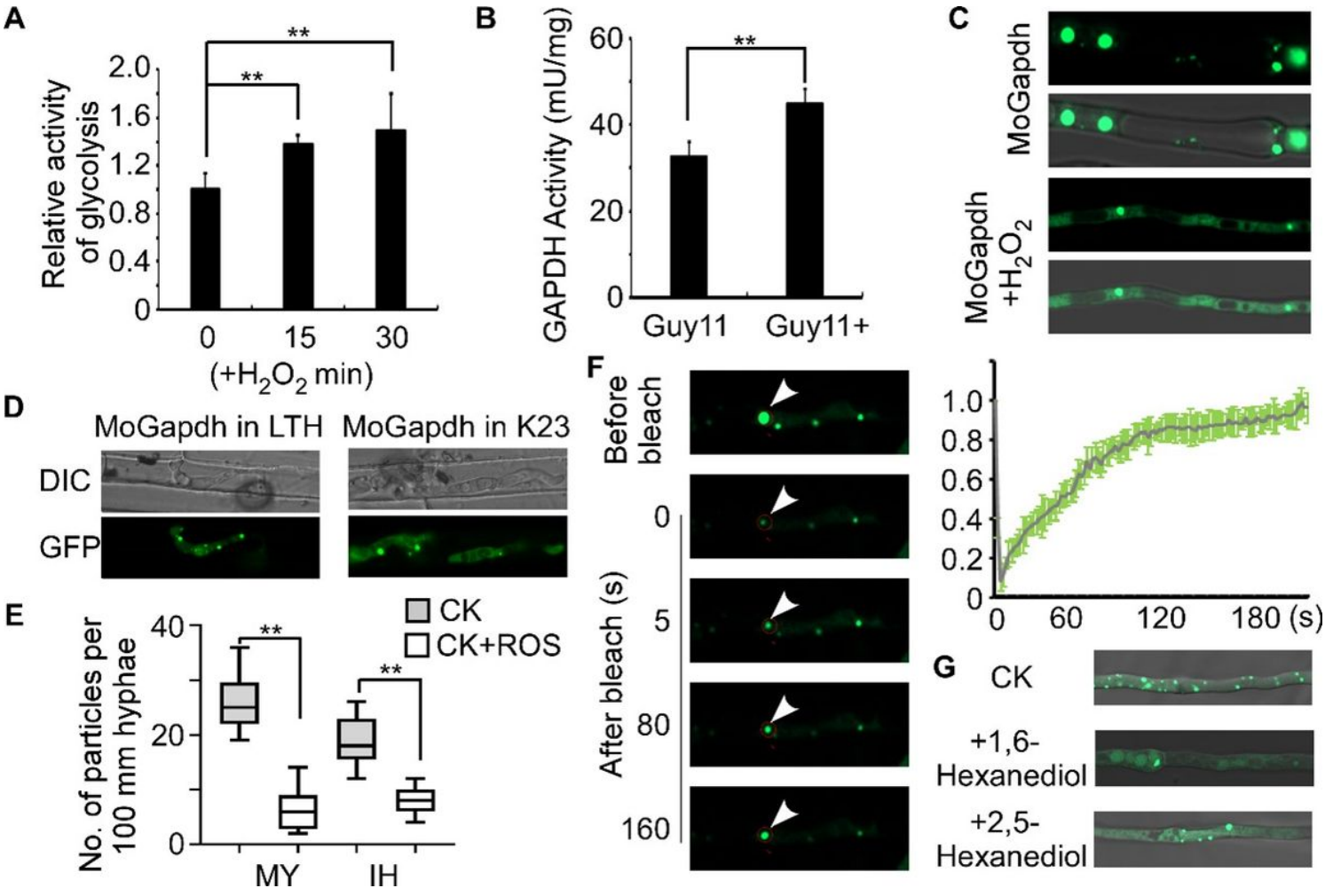

Figure 2

MoGapdh is dissociated from phase separation under ROS stress to supply energy for vesicle movement

(A) Total glycolysis activity was measured after 15- or 30-minute H_2O_2 treatment. "**", $P< 0.01$. (B) Total GAPDH activity was analyzed with H_2O_2 treatment for 30 minutes. "*, $P< 0.05$. (C) and (D) localization of

MoGapdh in mycelium and infection cells at 24 hpi. (E) Statistics of the particle per 100 μm hyphae. MY: mycelium, IH: infection hyphae. Error bars represent standard deviation, "**", $P < 0.01$. (F) Quantitative FRAP of MoGapdh. White arrow represents detected particles. The FRAP curves of MoGapdh-GFP localized regions, 20 regions from different cells were subjected to FRAP analysis for each strain. (G) Treatment of MoGapdh condensates by 1,6-hexanediol. Images showing condensates in mycelium under mock and 10% 1,6- hexanediol treatment for 30 mins. Bar = 5 μm. 2.5-hexanediol was used as the negative control.

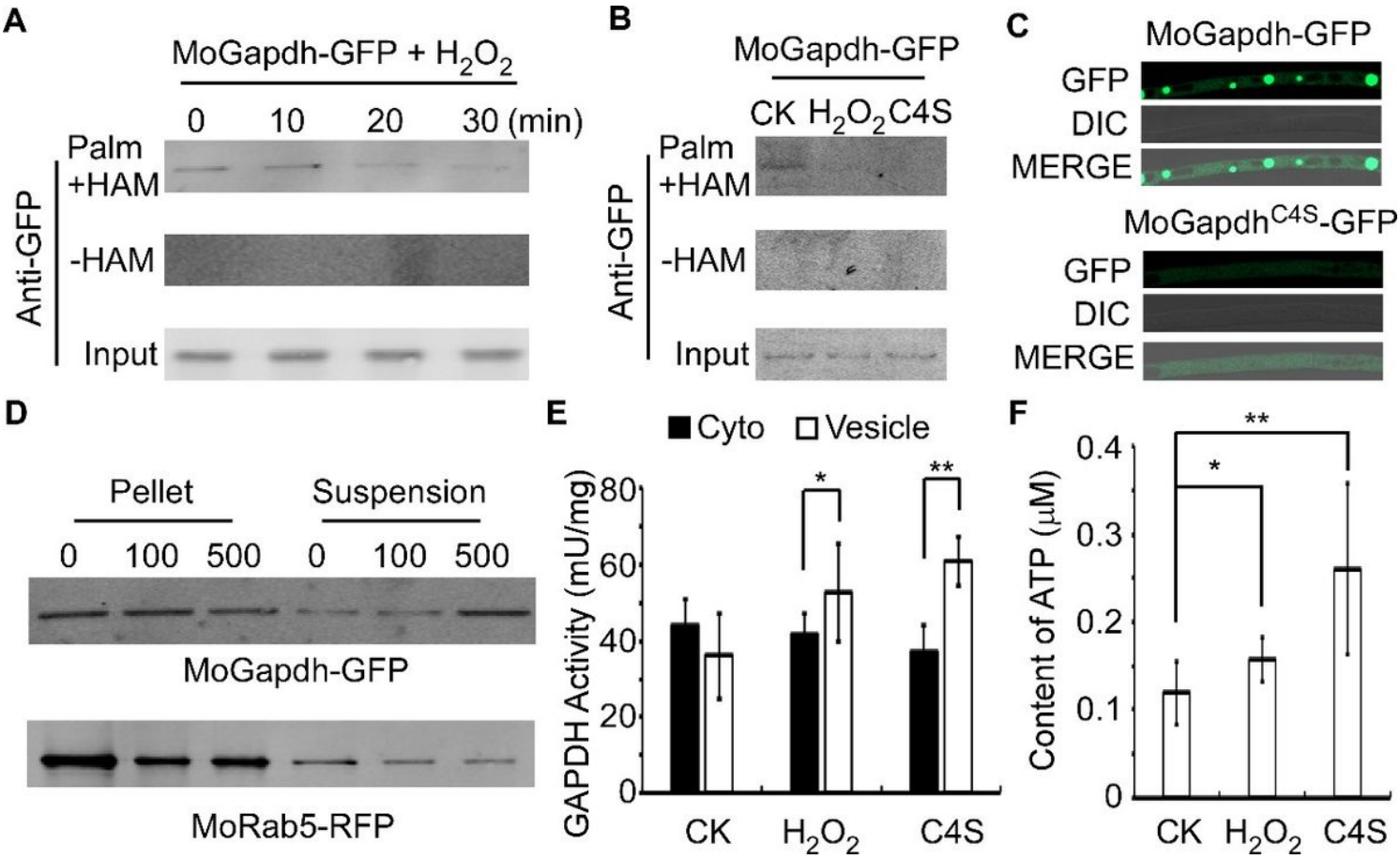

Figure 3

Palmitoylation of GAPDH is important for its phase separation

(A) Detection of MoGapdh palmitoylation in *M. oryzae* after ROS treatment. The palmitoylation levels were detected by an acyl-resin capture (acyl-RAC) assay. Palm- palmitoylated protein, HAM, hydroxylamine, for cleavage of the Cys-palmitoyl thioester linkages. Input represents the total protein. Experiments were repeated three times. (B) Detection of MoGapdh palmitoylation and its associated residue in *M. oryzae*. Sample treated with H_2O_2 for 30minutes was used as control. (C) Localization of MoGapdh and MoGapdh^{C4S} in mycelia. MoGapdh^{C4S}-GFP was observed by confocal fluorescence microscopy. Scale bars = 5μm. (D) Vesicles were prepared from MoGapdh-GFP/MoRab5-RFP and MoGapdh^{C4S}-GFP/MoRab5-RFP strains treated with different concentrations of salt as indicated. Free and vesicle-bound proteins were extracted and separated by SDS-PAGE, and the presence of MoGapdh

and MoRab5 was detected by Western blotting analysis using anti-GFP or anti-RFP antibodies. (E) The proteins of MoGapdh and its mutation were prepared from cytoplasm and vesicles which treated with H_2O_2 for 30 minutes. (F) After addition of GAP, NAD, ADP, and Pi, ATP production in the vesicle fraction was measured using a luciferin/luciferase kit. Three independent experiments were performed. Bars denote standard errors from three independent experiments. "*" $P< 0.05$, "**" $P< 0.01$ in this figure.

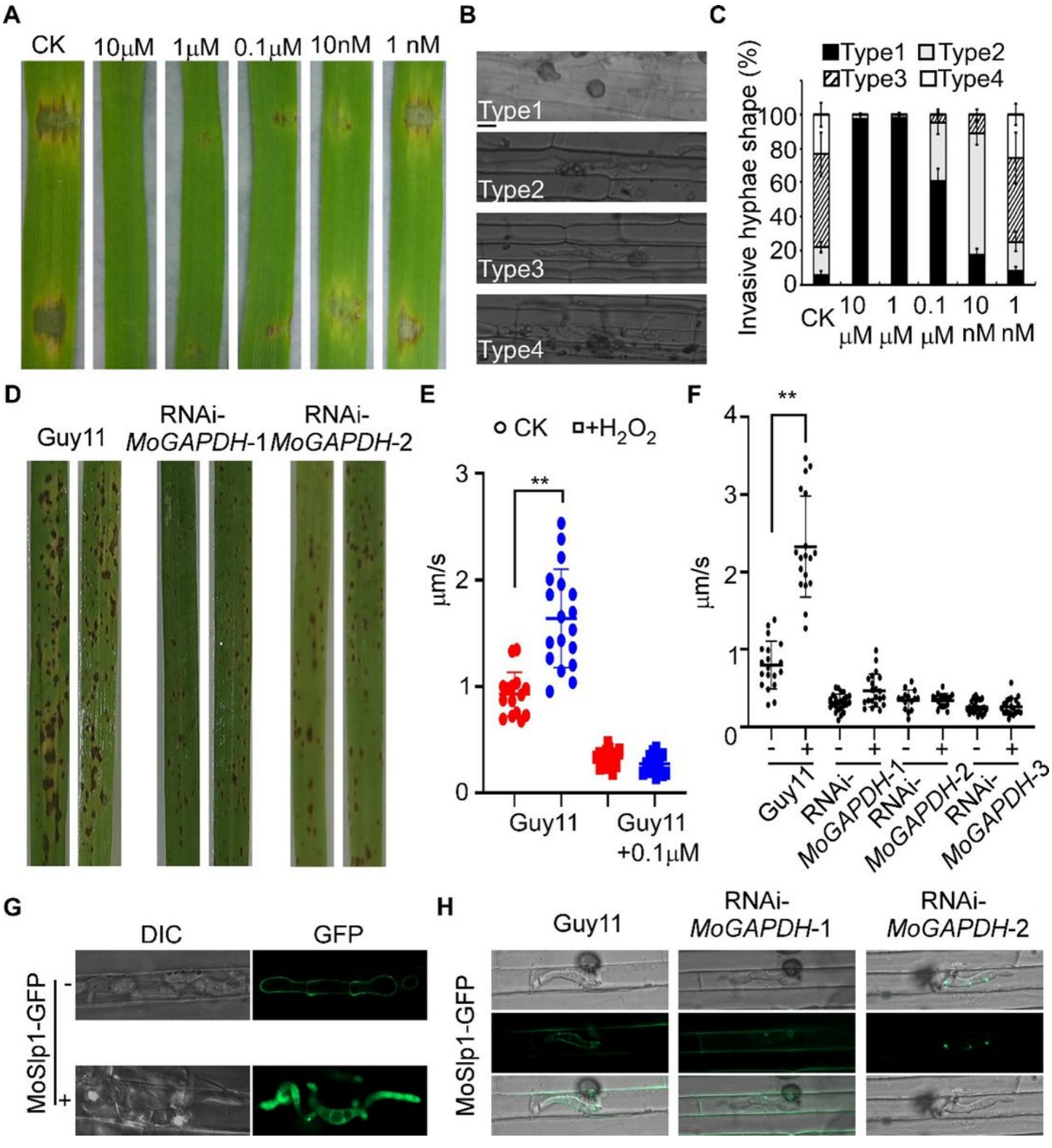

Figure 4

MoGapdh activity is important for the full virulence of *M. oryzae*

(A) Conidial suspensions (with or without IA) from Guy11 were dropped onto detached barley leaves. Photographs were taken at 5 dpi. (B and C) Conidial suspensions (with referred IA) were used to inject excised rice sheaths from 21-day-old CO-39 seedlings. 4 types of IH growth were observed after inoculating 24 hpi (1, one appressoria; 2, with primary invasive hypha; 3, IH secondary invasive hypha did not extend to neighboring plant cells; 4, invasive hypha extended into neighboring plant cells). Appressorium penetration sites were observed (n = 100). The experiment was repeated three times. Scale bar = 5 μm. (D) Conidial suspensions of RNAi-*MoGAPDH* strains were sprayed onto two-week-old rice seedlings (CO-39). Diseased leaves were photographed after 7 days of inoculation. (E) and (F) Movement of vesicles with 0.1 μM IA and in RNAi-*MoGAPDH* strains were calculated by Video Spot Tracker. (G) Fluorescence observation of rice leaf sheath cells injected with Guy11 (treated with 0.1 μM IA), which expressing MoSlp1. Bars=5 μm. (H) Fluorescence observation of rice leaf sheath cells injected with RNAi-*MoGAPDH* strains expressed MoSlp1. Asterisksindicate significant differences between the different strains ($P < 0.01$) in this figure.

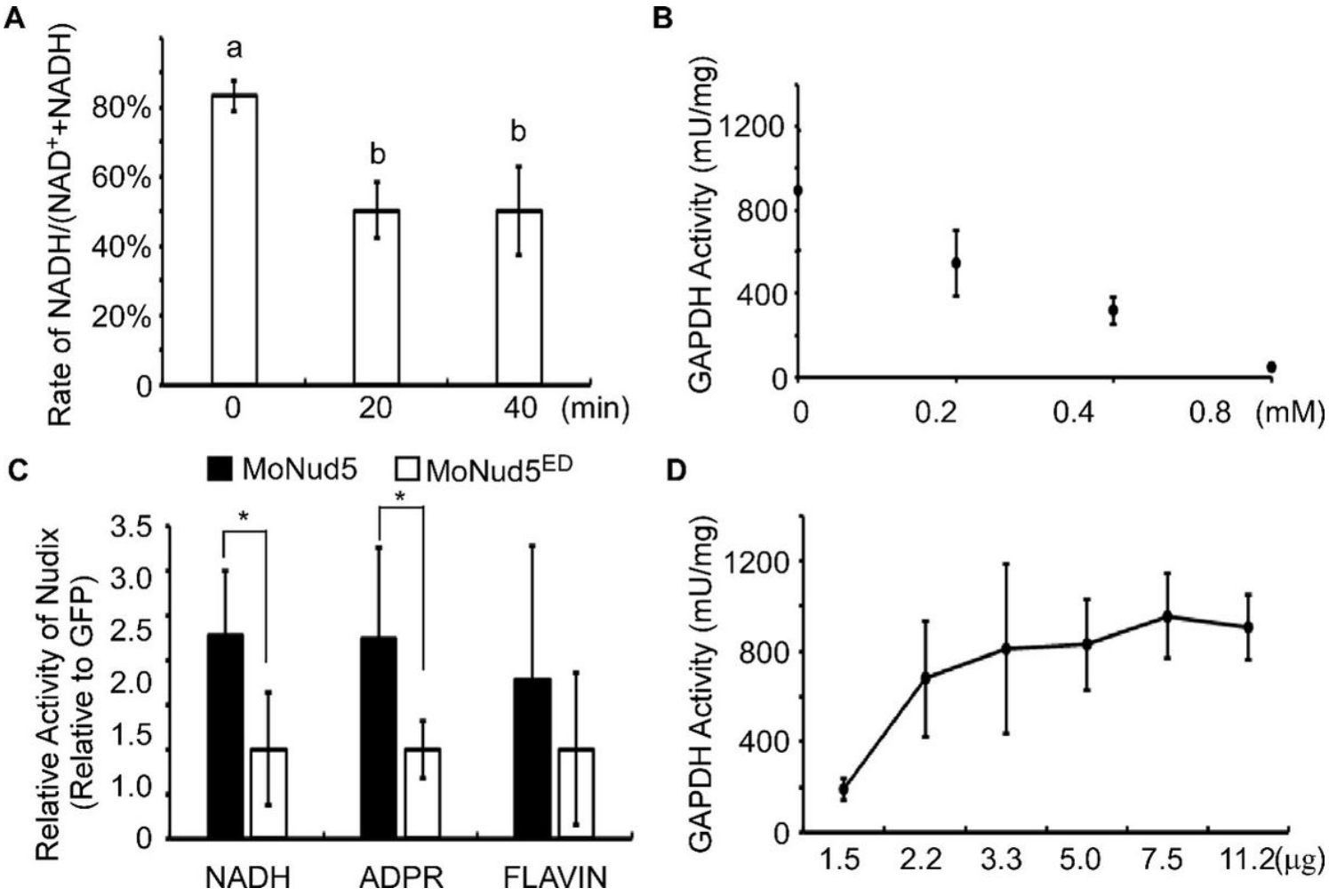

Figure 5

Excessive NADH inhibits the activity of MoGapdh

(A) Rates of NADH and NAD+ under stress. Mycelia were treated with H_2O_2 for 15 and 30 minutes. (B) NADH inhibited the activity of GAPDH. MoGapdh-GFP was extracted and incubated with NADH (mM) in a concentration gradient. Bars denote standard errors from three independent experiments. (C) Enzyme assays of purified MoNud5 and control proteins. MoNud5 functions as the Nudix hydrolase in *M. oryzae*. NADH, ADPR (ADP-ribose) and flavin mononucleotide (FMN) were used to evaluate the Nudix hydrolase. $MoNud5^{ED}$ represents to the enzyme activity center deletion mutant (deletion mutation from R104 to G111) (D) MoNud5 neutralizes the inhibition of NADH on the activity of MoGapdh. MoGapdh-GFP was extracted and co-incubated with 0.4 mM NADH and a concentration gradient of MoNud5 protein (μg). Bars denote standard errors from three independent experiments. “*” represent significant differences between the different strains ($P < 0.05$) in this figure.

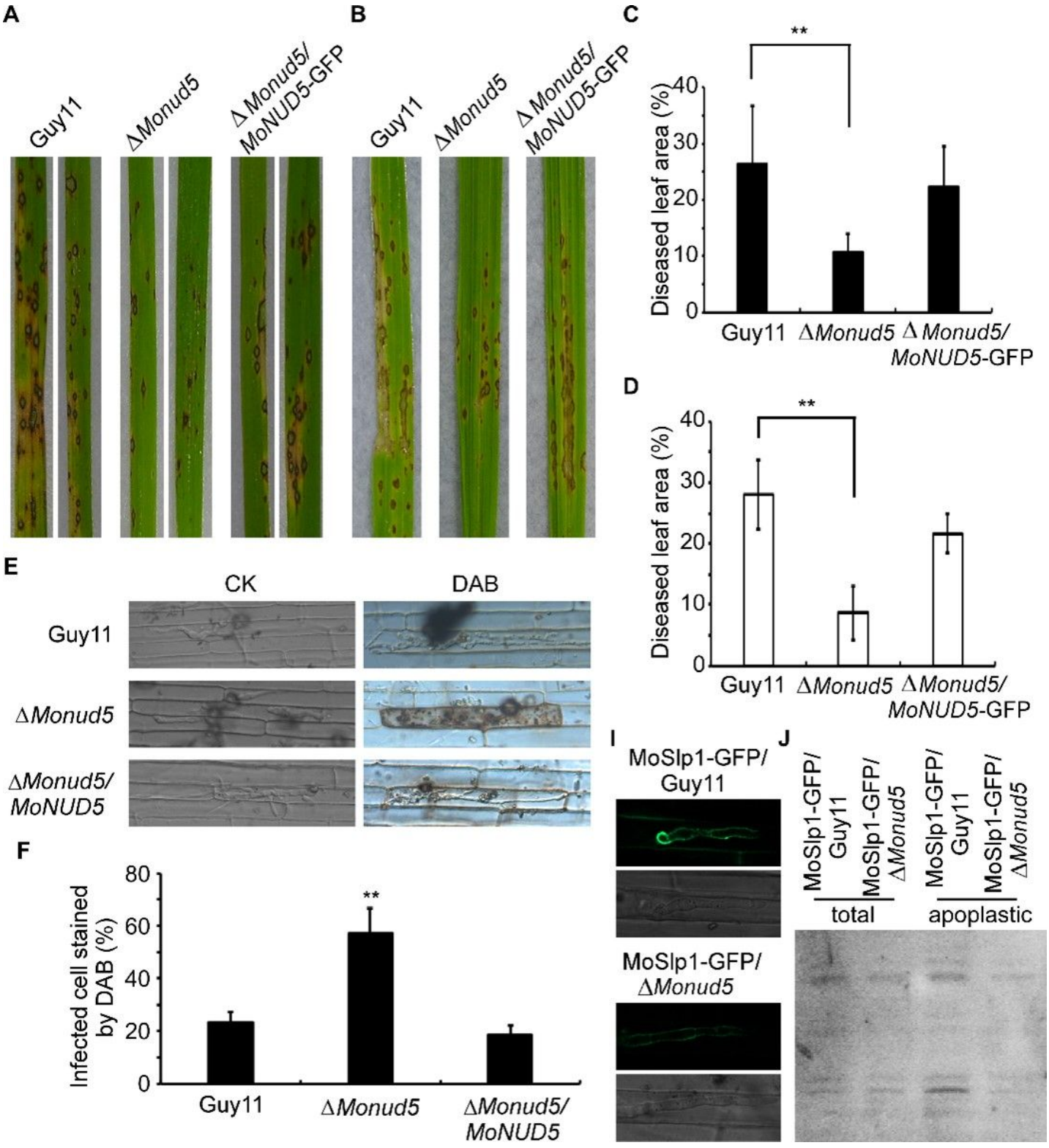

Figure 6

MoNud5 is important for the infection and full virulence of *M. oryzae*

(A and C) The pathogenicity assay on rice leaves. Conidial suspensions of strains were sprayed onto two-week-old rice seedlings (CO-39). Diseased leaves were photographed (A) and analyzed (C) after 7 days of inoculation. The percentage of lesion area was analyzed by Image J, and the results were presented as a

bar chart. (B and D) Conidial suspension of each strain was injected into leaf sheaths of 21-day-old rice seedlings (CO-39). Diseased leaves were photographed (B) and analyzed (D) 7 days after inoculation. (E and F) The infected cell stained by DAB. Three independent biological experiments were performed, with three replicates each time and yielded similar results in each independent biological experiment. (G) Fluorescence observation of rice leaf sheath cells injected with Guy11 or Δ*Monud5* expressed MoSlp1. (H) Total and apoplastic proteins were extracted from Guy11 or Δ*Monud5* expressed MoSlp1 strain and detected by Western blotting using the anti-GFP antibody. Error bars represent standard deviation, and asterisks represent significant difference between the different strains ($P < 0.01$) in this figure.

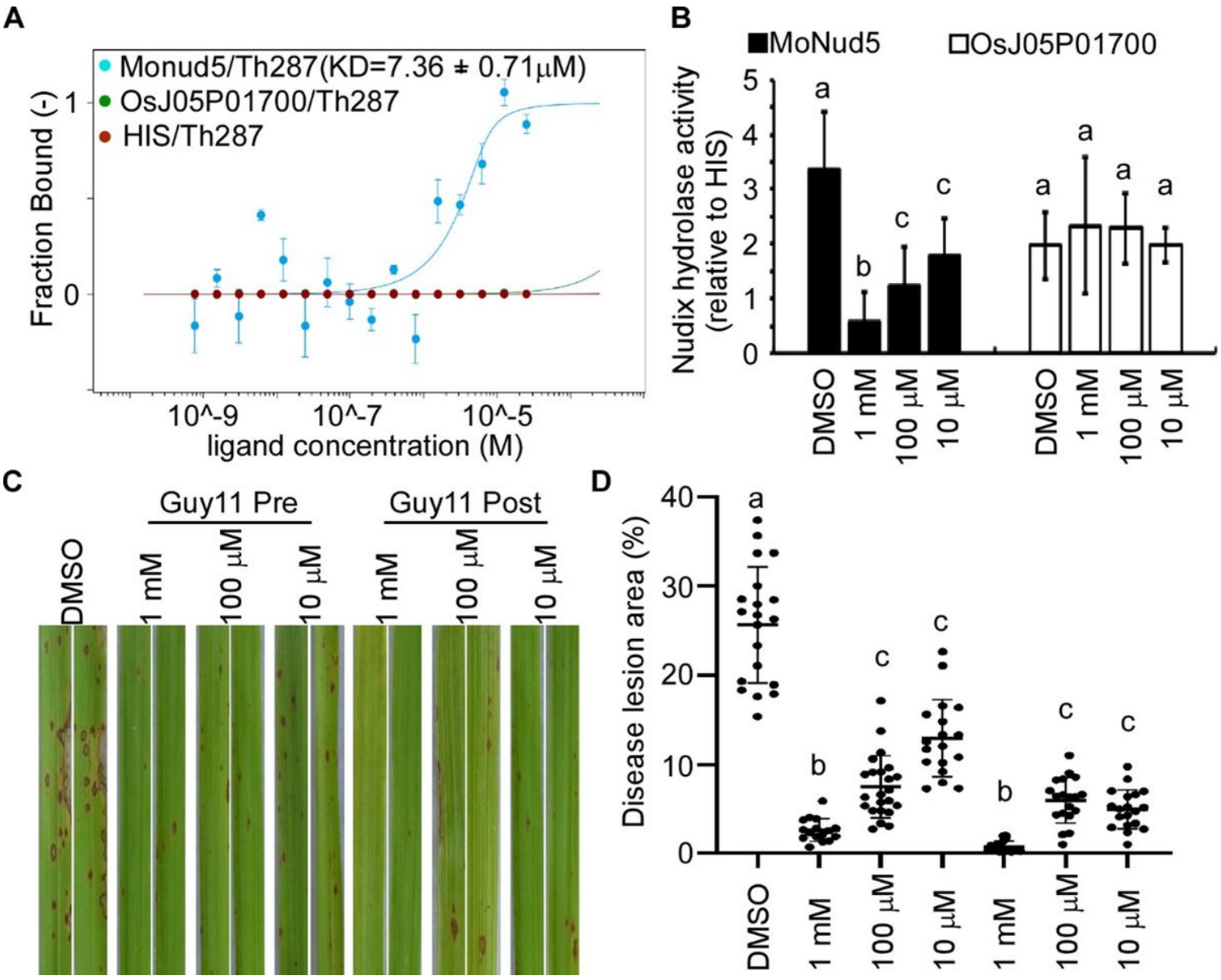

Figure 7

TH287 is effective against rice blasts

(A) TH287 exhibits a stronger MoNud5 binding affinity than OsJ05P01700 as assessed using microscale thermophoresis (MST). 10 μM MoNud5-HIS and OsJ05P01700-HIS was labeled by RED-NHS. The raw

data were integrated and fitted to a binding model using the MST analysis software. The recombinant proteins were contained in NT standard capillaries. The solid curve is the fit of the data points to the standard Kd-fit function. Kd, dissociation constant. (B) Both MoNud5-GFP (from *M. oryzae*) and OsJ05P01700-GFP (from *N. benthamiana*) proteins were extracted and purified. Proteins were incubated with different concentration of TH287. The Nudix hydrolase activity was measured using NADH as substrate. Bars denote standard errors from three independent experiments. (C and D) TH287 is effective against rice leaf blast. Rice leaves were sprayed with 1 mM, 100 μM and 10 μM compounds, 24 h pre-inoculation or post-inoculation with Guy11 spores. Diseased rice leaves were photographed after 7 days, blast disease lesion areas were quantified from infected leaves.

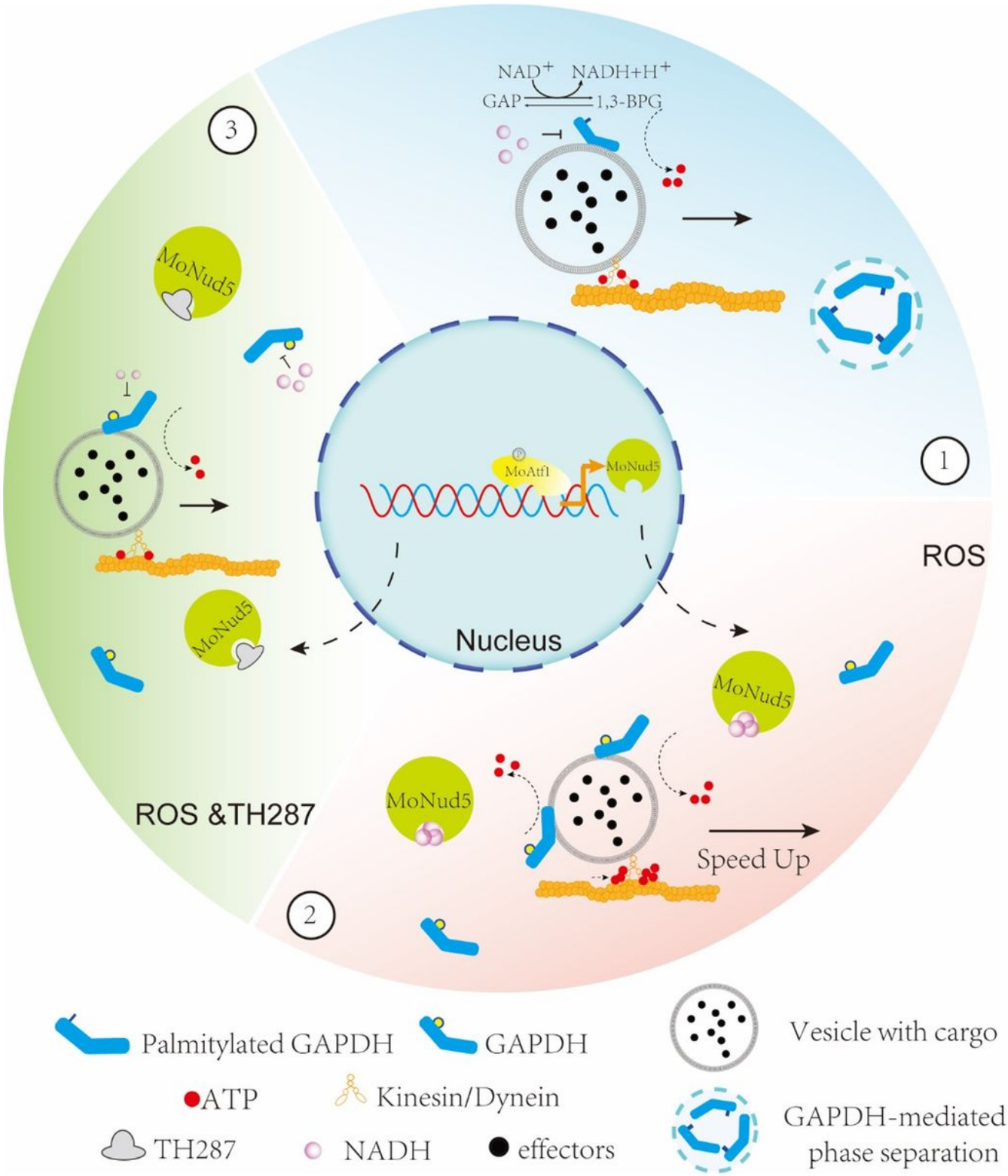

Figure 8

A proposed model depicting that glycolysis provides energy for vesicle trafficking and effector secretion in response to ROS stress

During the *M. oryzae*-rice interaction, rice cells perceive *M. oryzae* infection and induce ROS burst which in turn is sensed by *M. oryzae*. The recognition of host-induced ROS facilitates vesicle trafficking by

acquiring more energy from glycolysis. ROS inhibites the palmitoylation of GAPDH, leading to the dissociation of GAPDH-mediated phase separation which raises the GAPDH-pool in cytoplasm. More free MoGapdh accumulates around vesicle that contributes to the ATP generation to speed up trafficking. In this process, MoNud5 is up-regulated to control the concentration of NADH that liberates the activity of MoGapdh and thus the glycolysis. In addition, an inhibitor of Nudix hydrolase, TH287, specifically binds MoNud5 to suppress its function, which results in excessive NADH and subsequent a decreased activity of MoGapdh, to control *M. oryzae* infection.

Supplementary Files

This is a list of supplementary files associated with this preprint. Click to download.

- video1.avi
- video2.avi
- SupplementaryFigures.docx